



The crystal structure and redefinition of utahite

Owen P. Missen^{1,2} · Stuart J. Mills¹ · Michael S. Rumsey³ · Malcolm E. Back⁴ · Veronica E. Di Cecco⁴ · William D. Birch¹ · John Spratt⁵

Received: 27 October 2020 / Accepted: 11 March 2021 / Published online: 17 April 2021
© The Author(s), under exclusive licence to Springer-Verlag GmbH Austria, part of Springer Nature 2021

Abstract

Utahite was first described in 1997 based mainly on powder X-ray diffraction data and electron microprobe data. No crystal structure was reported. The re-examination of utahite using single-crystal X-ray diffraction and electron microprobe analysis has shown that utahite contains essential Mg, along with Cu, Zn, Te, O and H. The missing MgO was originally attributed to additional H₂O. The redefinition of utahite to MgCu²⁺₄Zn₂Te⁶⁺₃O₁₄(OH)₄·6H₂O from Cu²⁺₅Zn₃(Te⁶⁺O₄)₄(OH)₈·7H₂O has been accepted by the IMA–CNMNC, Proposal 20-C. Utahite is triclinic, crystallising in $P\bar{1}$ with the unit-cell parameters $a = 5.6831(4)$ Å, $b = 8.7793(6)$ Å, $c = 9.9818(9)$ Å, $\alpha = 95.415(7)^\circ$, $\beta = 104.129(7)^\circ$, $\gamma = 90.098(6)^\circ$ and $V = 480.65(7)$ Å³, in good agreement with the original study. Utahite features a new framework arrangement of Cu φ_6 octahedra, Zn φ_4 tetrahedra and Te φ_6 octahedra (where $\varphi = O$ or OH), with Mg(H₂O)₆ octahedra occupying the channel space. Two-thirds of the Te sites form Te⁶⁺₂O₁₀ dimers and one third form [Te⁶⁺O₄(OH)₂]⁴⁻ octahedra, spatially separated from other Te⁶⁺ sites. Although unique, the structural framework of utahite is similar to that of leisingite, with both minerals having layers composed of Cu φ_6 and Te φ_6 octahedra with Mg(H₂O)₆ octahedra in the interlayer space; however leisingite does not contain Zn. New Raman spectroscopic data is also reported for utahite.

Keywords Utahite · Tellurate · Tellurium oxysalt · Crystal structure · Empire mine, Cochise County, Arizona, USA · Centennial Eureka mine, Juab County, Utah, USA

Introduction

Nearly two hundred tellurium (Te) minerals have been described, around half of which contain oxygen. Though generally rare, the Te oxysalt minerals are remarkably chemically and structurally diverse (Christy et al. 2016; Missen et al.

2020a). Utahite was first described by Roberts et al. (1997a) with the formula Cu₅Zn₃(Te⁶⁺O₄)₄(OH)₈·7H₂O, one in a series of copper–tellurium oxysalts described from the Centennial Eureka mine in Juab County, Utah, USA (39°56′36″N, 112°7′19″W). The Centennial Eureka mine produced copper (Cu), silver (Ag) and gold (Au), resulting in the accumulation of large dumps during its main operation (most production ceased almost a century ago). It was not until these dumps were removed in 1991 to process them for their Au content decades later that the rich assemblage of Cu–Te⁶⁺–O minerals was exposed (Roberts et al. 1997a). Roberts and co-workers described six new Cu–Te⁶⁺–O minerals between 1994 and 1997, namely mc Alpineite (Roberts et al. 1994), frankhawthorneite (Roberts et al. 1995; Grice and Roberts 1995), jensenite (Roberts et al. 1996a; Grice et al. 1996), leisingite (Roberts et al. 1996b; Margison et al. 1997), utahite (Roberts et al. 1997a) and juabite (Roberts et al. 1997b). Mc Alpineite has a cotype locality, namely the eponymous Mc Alpine mine in Tuolumne County, Northern California, while the other five were described from the Centennial Eureka mine alone. Eureka dumpite was noted at the same

Editorial handling: M. A. T. M. Broekmans

✉ Owen P. Missen
omissen@museum.vic.gov.au

¹ Geosciences, Museums Victoria, GPO Box 666, Melbourne 3001, Victoria, Australia

² School of Earth, Atmosphere and Environment, Monash University, 9 Rainforest Walk, 3800 Clayton, Victoria, Australia

³ Department of Earth Sciences, Natural History Museum, Cromwell Road, London SW7, UK

⁴ Department of Natural History, Mineralogy, Royal Ontario Museum, 100 Queen's Park, Toronto, Ontario M5S 2C6, Canada

⁵ Department of Core Research Laboratories, Natural History Museum, Cromwell Road, London SW7 5BD, UK

time but was not described for over a decade (Pekov et al. 2010, 2011). Structure determinations exist for all of these minerals except for utahite and eurekaumpite. Here we present structural and spectroscopic data from an exceptionally well-crystallised specimen of utahite. This structural determination forms part of our broader study on the re-examination of all Te secondary minerals without known crystal structures.

Specimen descriptions

The portion of the type specimen of utahite (from the Centennial Eureka mine) examined in this study consists of an aggregate of utahite laths, sub-mm in size, embedded in a resin block, stored in the collections of the Natural History Museum, London, specimen number BM 1994,99. This was the portion of the utahite cotype specimens used in the original study (Roberts et al. 1997a) for the electron microprobe work and an attempted reflectance study, subsequently referred to as the NHM cotype in this paper. The remaining cotype material consists of three specimens and an SEM stub stored in the National Mineral Collection at the Geological Survey of Canada, Ottawa, catalogue number 67,415 (Roberts et al. 1997a).

An additional specimen of utahite was used for structural determination, and as such is now designated as an additional cotype specimen for utahite, from a new cotype locality. The specimen is from the Empire mine, Cochise County, Arizona, USA. It is stored in the collections of the Royal Ontario Museum (ROM), Toronto, with specimen number M59810 and was obtained by the ROM from Peter Megaw. Utahite forms several sprays of light blue crystals on this specimen along with very dark green (almost black) khinite and a variety of light and dark green crusts of poorly crystallised Cu–Te–O oxidation products (Fig. 1). Utahite crystals may reach 0.3 mm in length but are usually 0.1 mm long. Several spatially-separated crystal sprays cover almost 1 cm² of the sample.

Electron probe microanalysis (EPMA)

Chemical analytical data for the NHM cotype specimen (BM 1994,99) were collected on a Cameca SX100 Electron Microprobe (WDS mode, 20 kV, 20 nA, 1 µm beam diameter and PAP matrix correction) at the Imaging and Analysis Centre, Core Research Laboratories, Natural History Museum, London. The following elements were also analysed for but found to be below detection limit: Si, S, Ti, Mn, Fe, As, Se, Ag, Pb and Bi.

Chemical analytical data on the additional cotype (ROM specimen M59810) were performed on a JXA-8530 F Field Emission Electron Microprobe (WDS mode, 15 kV, 5 nA,

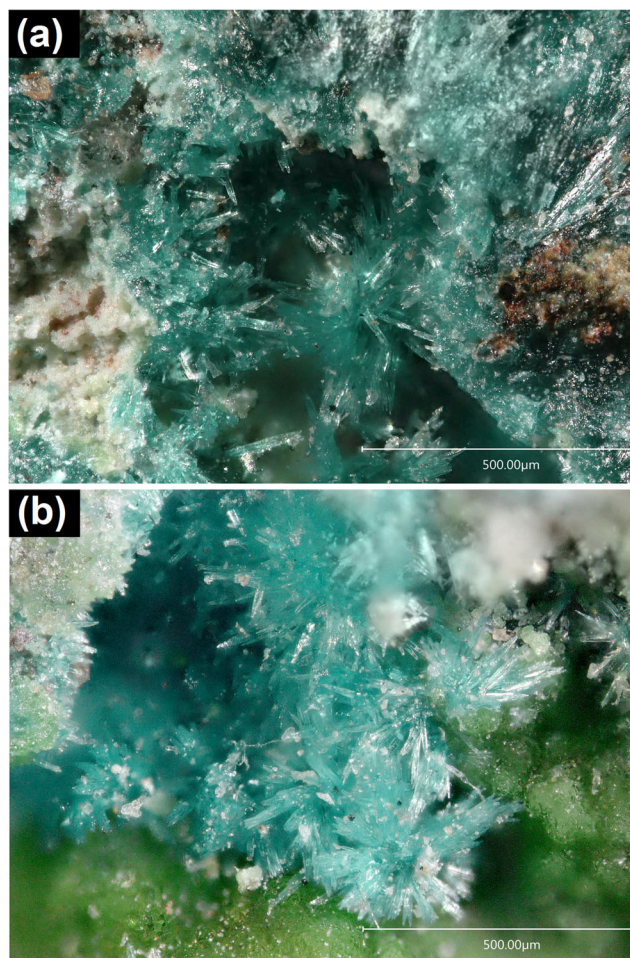


Fig. 1 Optical images of utahite crystal clusters on an unknown green mineral, probably a poorly crystallised copper tellurite (ROM utahite specimen, M59810)

20 µm beam diameter and PAP matrix correction), at the School of Earth Sciences, University of Melbourne, Australia. Fe was also analysed for but found to be below detection limit.

Note that although the totals for the two analyses differ by 10 %, the elemental ratios obtained are nearly identical. The difference in totals probably arises from the different conditions under which the two data sets were generated, a consequence of the analyses for the two specimens being performed on different instruments. Results, including the standards used for each EPMA data collection, are listed in Table 1. The empirical formulae for the NHM and ROM specimens (based on 24 O + OH anions *pfu*, with H calculated based on the crystal structure) are Mg_{0.96}Na_{0.12}Ca_{0.05}Cu_{3.67}Al_{0.04}Zn_{2.19}Te_{2.86}Sb_{0.04}P_{0.02}O₂₄H_{16.13} and Mg_{1.01}Na_{0.12}Cu_{3.78}Zn_{2.05}Te_{2.98}Sb_{0.01}O₂₄H_{16.13} respectively. Substitutions are necessary to evenly fill the metal atom sites in the crystal structure, as the elemental totals from EPMA are not in integer ratios. These substitutions are Zn and Na for Cu (in different Cu-dominant sites), and Sb for Te in both specimens, along with Ca for Mg, and Al for Te in the NHM cotype

Table 1 EPMA data for the two utahite specimens analysed, including Roberts et al. (1997a) for comparison

Oxide	BM 1994,99 specimen (NHM, London) 6 analyses				M59810 specimen (ROM additional cotype) 5 analyses				Roberts et al. analysis (1997a)
	wt%	Average	Range	St. Dev	Standard	Average	Range	St. Dev	
Na ₂ O	0.34	0.29–0.39	0.04	jadeite	0.29	0.27–0.32	0.02	jadeite	ND
MgO	3.43	3.28–3.56	0.11	forsterite	3.22	3.16–3.33	0.07	periclase	ND
CaO	0.23	0.18–0.27	0.03	wollastonite	NA				ND
CuO	25.88	24.96–27.14	0.83	chalcopyrite	23.84	23.54–24.25	0.34	Cu metal	25.76
ZnO	15.80	14.76–17.02	0.75	ZnS <i>syn.</i>	13.26	12.96–13.56	0.25	Zn metal	15.81
Al ₂ O ₃	0.17	0.15–0.22	0.04	corundum	NA				ND
P ₂ O ₅	0.11	0.07–0.17	0.04	apatite	NA				ND
Sb ₂ O ₅	0.54	0.42–0.80	0.13	Sb metal	0.15	0.09–0.19	0.04	Sb metal	ND
TeO ₃	44.37	42.95–45.15	0.79	TeO ₂ <i>syn.</i>	41.44	41.25–41.68	0.16	Te metal	45.47
H ₂ O	12.85*				11.50*				12.96**
Total	103.73				93.70				100.00

NA: not analysed (below 0.1 wt% based on an earlier SEM-EDX scan). ND: not detected (by Roberts et al. using wavelength-dispersive scan).

*Calculated based on the crystal structure. ** Calculated by difference

The bold text highlights the average values to make them stand out from range and standard deviations

specimen. It is worth noting that the calculated levels of Na in utahite may be affected by the Zn contents, with a peak overlap of emitted X-rays known for Na (Na K_{α} 1.041 keV) and Zn (Na L_{α} 1.012 keV). The grouped empirical formulae are $(\text{Mg}_{0.96}\text{Ca}_{0.05})_{\Sigma 1.01}(\text{Cu}_{3.67}\text{Zn}_{0.20}\text{Na}_{0.12})_{\Sigma 3.99}\text{Zn}_{1.99}(\text{Te}_{2.86}\text{Sb}_{0.04}\text{Al}_{0.04}\text{P}_{0.02})_{\Sigma 2.96}\text{O}_{13.87}(\text{OH})_{4.13} \cdot 6\text{H}_2\text{O}$ and $\text{Mg}_{1.01}(\text{Cu}_{3.78}\text{Na}_{0.12}\text{Zn}_{0.07})_{\Sigma 3.97}\text{Zn}_{1.98}(\text{Te}_{2.98}\text{Sb}_{0.01})_{\Sigma 2.99}\text{O}_{13.87}(\text{OH})_{4.13} \cdot 6\text{H}_2\text{O}$, respectively. The site-filling scheme was determined using the electron microprobe data in conjunction with structural considerations (see below). The ideal formula is $\text{MgCu}^{2+}_4\text{Zn}_2\text{Te}^{6+}_3\text{O}_{14}(\text{OH})_4 \cdot 6\text{H}_2\text{O}$, requiring MgO 3.38, CuO 26.69, ZnO 13.65, TeO₃ 44.19 and H₂O 12.09, total 100 wt%.

Raman spectroscopy

Micro-Raman spectra of randomly oriented single crystals of utahite (Fig. 2) from the ROM additional cotype specimen were collected with a Horiba LabRAM ARAMIS micro-Raman spectrometer at the Royal Ontario Museum in Toronto, Canada. The 532 nm excitation line of a 50 mW Ar-ion laser was focused with a 50 LWD (0.5) objective lens created a 1.3 μm spot on the sample surface. Laser power was filtered to 25 % and a 400 μm slit, 100 μm hole, and 1200 lines/mm grating were used for data collection. An early data collection with laser power filtered to 50 % burned the sample.

Fig. 2 The Raman spectrum of utahite (from ROM M59810, additional cotype specimen)

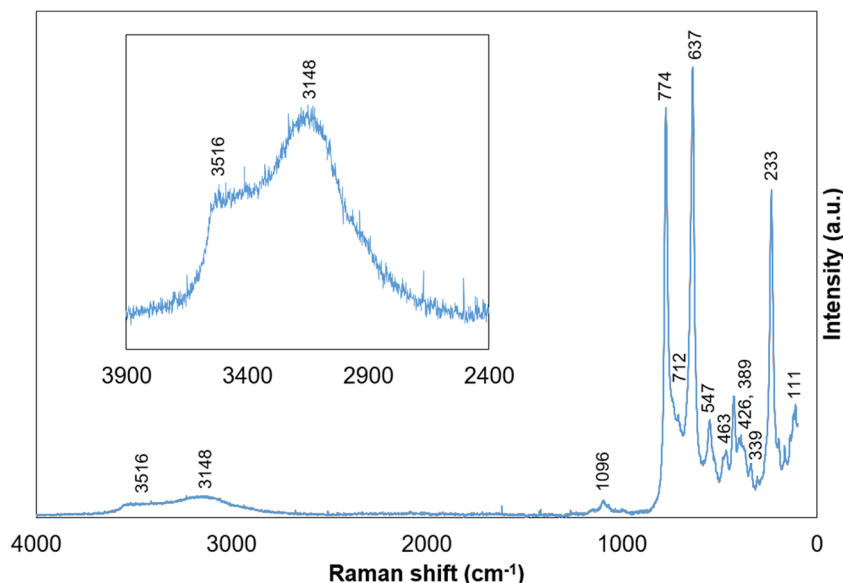


Table 2 Comparison of calculated powder X-ray diffraction (PXRD) pattern of utahite (ROM M59810) from the Empire mine with the observed NHM cotype specimen (BM 1994,99) PXRD pattern. Cutoffs: averaged $I > 5$ and $d > 2 \text{ \AA}$

M59810 ROM additional cotype (this study)			BM 1994, 99 NHM cotype (Roberts et al. 1997a)		
I_{calc}	$d_{\text{calc}}, \text{ \AA}$	hkl	I_{meas}	$d_{\text{meas}}, \text{ \AA}$	
100	9.633	0 1 0	100	9.638	
34	8.737	1 0 0	50	8.736	
28	6.812	$\bar{1}$ 1 0	40	6.862	
26	6.178	1 1 0	40	6.172	
12	5.509	0 0 1	30	5.488	
98	4.817	0 2 0	100	4.841	
9	4.369	2 0 0	20	4.380	
14	4.134	$\bar{2}$ 1 0	40	4.152	
11	3.994	$\bar{1}$ 1 1	20	3.995	
20	3.840	2 1 0	40	3.822	
1, 5	3.211, 3.185	0 3 0, $\bar{2}$ 1 1	10	3.203	
18	3.114	$\bar{1}$ 3 0	40	3.129	
7	3.023	$\bar{1}$ 3 $\bar{1}$	10	3.030	
5	2.986	2 1 1	5	2.978	
10, 10	2.923, 2.912	3 0 0, 1 3 0	30	2.912	
9	2.839	0 1 $\bar{2}$	20	2.827	
33	2.755	0 0 2	60	2.747	
15	2.693	0 2 $\bar{2}$	30	2.681	
10, 11	2.603, 2.594	$\bar{3}$ 0 1, $\bar{3}$ 1 $\bar{1}$	45	2.600	
10	2.531	3 1 $\bar{1}$	10	2.520	
11, 17	2.474, 2.464	3 0 2, $\bar{3}$ 2 $\bar{1}$	40	2.478	
4	2.408	0 4 0	20	2.409	
8	2.347	$\bar{1}$ 3 $\bar{2}$	20	2.348	
13	2.318	3 2 $\bar{1}$	25	2.307	
2, 2	2.289, 2.263	1 3 $\bar{2}$, $\bar{3}$ 2 1	5	2.272	
5	2.223	$\bar{3}$ 3 $\bar{1}$	3	2.241	
5	2.211	$\bar{2}$ 1 2	3	2.206	
17	2.173	0 2 2	40	2.165	
6	2.121	2 1 2	5	2.116	
3	2.089	4 1 0	20	2.081	
5	2.061	2 3 $\bar{2}$	10	2.048	

Data was collected for a total of 1200 s in the spectral range 4000 to 100 cm^{-1} , in 30 s intervals \times 10 iterations, over 4 windows. The wavenumber accuracy was $\pm 1 \text{ cm}^{-1}$. The instrument was calibrated with a Si standard (521 cm^{-1}).

Between 1000 and 100 cm^{-1} , the spectrum confirms the presence of $\text{Te}^{6+}\text{-O}$ bonds. Two strong peaks, one centred on 774 cm^{-1} and the other on 637 cm^{-1} , are attributed to the symmetric ν_1 stretches of the two $\text{Te}^{6+}\text{-O}$ environments, namely $\text{Te}^{6+}\text{O}_4(\text{OH})_2$ octahedra and $\text{Te}^{6+}_2\text{O}_{10}$ dimers. Additionally, the 774 cm^{-1} peak has a shoulder at 712 cm^{-1} , attributable to the antisymmetric ν_3 stretching mode of $\text{Te}^{6+}\text{-O}$ bonds. Compared to other minerals containing $\text{Te}^{6+}_2\text{O}_{10}$ dimers, the mineral eckhardite (Kampf et al. 2013) has major Raman peaks at 729 and 692 cm^{-1} , while thorneite (Kampf et al. 2012) has major peaks at 833 cm^{-1} and 710 cm^{-1} with a shoulder at 670 cm^{-1} .

The utahite peak at 1096 cm^{-1} may be attributable to minor phosphate (as detected in the NHM cotype specimen), probably occupying channel space. The region below 600 cm^{-1} contains bands attributable to H_2O libration modes, Te-O bending modes and vibrations of the Cu- and Zn-centred polyhedra, as well as lattice modes. The strongest of these are well-defined peaks at 547 cm^{-1} (weak, probably a H_2O libration mode), 426 cm^{-1} (somewhat weak) and 233 cm^{-1} (moderately strong).

Between 4000 and 2000 cm^{-1} (Fig. 2, inset), the Raman spectrum confirms the presence of O-H bonds, with a broad maximum formed from the overlap of at least two peaks, indicating two distinct average O-H bond lengths. The peak centred on 3148 cm^{-1} is sharper, while the shoulder peak centred on 3516 cm^{-1} and extending towards 3600 cm^{-1} is broader. Using the correlation curve of Libowitzky (1999), the

Table 3 Crystallographic information relating to data collection and refinement of utahite

Crystal data	
Ideal Chemical Formula	Mg(Cu ²⁺ _{3.78} Na _{0.12} Zn _{0.10}) _{Σ4} Zn ₂ (Te ⁶⁺ _{2.99} Sb ⁵⁺ _{0.01}) _{Σ3} O _{13.87} (OH) _{4.13} ·6H ₂ O
Crystal system, Space group	Triclinic, <i>P</i> $\bar{1}$
Temperature (K)	100.00(10)
<i>a</i> , <i>b</i> , <i>c</i> (Å)	5.6831(4), 8.7793(6), 9.9818(9)
α , β , γ (°)	95.415(7), 104.129(7), 90.098(6)
<i>V</i> (Å ³)	480.65(7)
<i>Z</i>	1
Calculated density (g cm ⁻³)	4.046
Radiation type and wavelength (Å)	Mo <i>K</i> _α , λ=0.71073
μ (mm ⁻¹)	11.301
Crystal dimensions (mm)	0.020 × 0.020 × 0.100
Reflections for cell refinement	2284, 3.0210–30.8810 ° θ
Data Collection	
Crystal description	Blue needle
Diffractometer	Synergy diffractometer (Rigaku Oxford Diffraction)
θ (°) range	2.331–26.368
Indices range of <i>h</i> , <i>k</i> , <i>l</i>	<i>h</i> : ± 7, <i>k</i> : ± 10, <i>l</i> : -11 to 12
Absorption correction	Multi-scan ABSPACK
<i>T</i> _{max} , <i>T</i> _{min}	0.44325, 1.00000
No. of measured, independent and observed [<i>I</i> > 2σ(<i>I</i>)] reflections	5640, 1614, 1356
<i>R</i> _{int}	0.0959
Data completeness to 26.368° θ (%)	83.3
Refinement	
Number of reflections, parameters, restraints	1614, 95, 0
<i>R</i> ₁ [<i>F</i> ² > 2σ(<i>F</i> ²)], <i>R</i> ₁ (all)	0.1111, 0.1261
<i>wR</i> ₂ [<i>F</i> ² > 2σ(<i>F</i> ²)], <i>wR</i> ₂ (all)	0.2843, 0.2962
<i>GoF</i> (<i>F</i> ²)	1.092
$\Delta\rho_{\min}$, $\Delta\rho_{\max}$ (e Å ⁻³)	-5.53, 6.94

two mean H-bond donor–acceptor O⋯O distances in utahite are 2.92 Å and 2.69 Å. Above-background Raman intensity is observed between 2800 and 3600 cm⁻¹, thus a spread of O⋯O values may be expected. Utahite contains two OH and three H₂O groups, meaning that many O⋯O distances (see also Table 4) are observed in the utahite crystal structure including OW1⋯O8 (2.79 Å) and OW2⋯O3 (3.09 Å). Further variation in O⋯O values is expected as the OW sites are more mobile than O or OH sites. Further discussion of a hydrogen-bonding network is provided below.

Single crystal X-ray diffraction (SCXRD)

Experimental

The single crystal X-ray diffraction experiment was carried out on a Synergy diffractometer (Rigaku Oxford Diffraction) at the

School of Chemistry, University of Melbourne, Australia, using graphite-monochromated Mo*K*_α radiation (50 kV and 1 mA). The refined single-crystal X-ray diffraction pattern (details below) was used to generate a powder X-ray diffraction pattern, which was compared to the PXRD pattern reported for type utahite (Table 2) by Roberts et al. (1997a). The close match between the two PXRD patterns for both *d* spacings and measured intensities show that the studied sample of utahite is essentially identical in structure to type utahite.

A detailed search for the highest quality single crystals of utahite found that all crystals of utahite examined are twinned, with some overlapping reflections from the individual components. For this reason, reflections were placed into HKLF4 (reflections for one twin domain only) and HKLF5 (reflections for both twin domains) files. The refinement of the structure was performed using the HKLF4 dataset, with overlapping reflections excluded. Refinement using data from both twin domains (HKLF5) yielded a poorer quality dataset with an unacceptably

Table 4 Fractional atom coordinates, occupancies and displacement parameters for the atomic sites of utahite

Atom	x/a	y/b	z/c	U_{eq}	U^{11}	U^{22}	U^{33}	U^{23}	U^{13}	U^{12}
Te1	-0.0036(3)	0.32478(16)	-0.00712(16)	0.0071(5)	0.0065(9)	0.0019(9)	0.0137(9)	0.0014(6)	0.0040(6)	0.0029(6)
Te2*	1	0	½	0.0114(6)	0.0114(12)	0.0077(11)	0.0150(13)	0.0015(8)	0.0032(9)	0.0022(9)
Cu1*	0.5053(5)	0.1674(3)	-0.0013(3)	0.0057(7)	0.0045(16)	0.0025(16)	0.0117(16)	0.0010(11)	0.0050(12)	0.0025(11)
Cu2	½	½	0	0.0066(9)	0.004(2)	0.003(2)	0.013(2)	0.0007(15)	0.0036(16)	0.0016(15)
Cu3*	½	0	½	0.0090(10)	0.008(2)	0.009(2)	0.010(2)	-0.0003(17)	0.0011(17)	-0.0004(17)
Zn1	0.1206(5)	0.0231(3)	0.1816(3)	0.0093(7)	0.0089(15)	0.0054(14)	0.0139(15)	0.0019(11)	0.0031(11)	0.0017(10)
Mg1	½	½	½	0.016(3)						
O1	0.431(3)	0.016(2)	0.1201(19)	0.011(4)						
O2	0.055(3)	0.176(2)	-0.1383(18)	0.010(4)						
O3	1.044(4)	0.211(2)	0.589(2)	0.015(4)						
O4	0.201(3)	0.052(2)	0.3814(18)	0.009(3)						
O5	-0.076(4)	0.190(2)	0.113(2)	0.015(4)						
O6	0.645(4)	0.328(2)	-0.089(2)	0.014(4)						
O7	0.048(3)	0.4937(19)	-0.1182(18)	0.006(3)						
O8	0.345(3)	0.340(2)	0.0789(19)	0.010(4)						
O9	0.702(3)	0.049(2)	0.3815(19)	0.011(4)						
OW1	0.387(4)	0.643(2)	0.646(2)	0.017(4)						
OW2	0.862(4)	0.555(2)	0.607(2)	0.022(4)						
OW3	0.503(4)	0.682(2)	0.377(2)	0.017(4)						

*Te2/Sb1 occupancy fixed at 99:1 (free-variable refined on Te2 occupancy is < 1, indicating presence of a lighter element i.e. Sb), Cu1:Zn1 occupancy fixed at 95:5 (free-variable refined on Cu1 occupancy is > 1, indicating presence of a heavier element i.e. Zn) and Cu3:Na1 occupancy fixed at 88:12 (free-variable refined on Cu3 occupancy is > 1, indicating presence of a lighter element i.e. Na). Ratios then fixed to best match the EPMA data

high R_{int} value. In addition, refinement using the HKLF5 dataset yielded larger residual electron density peaks than those obtained using the HKLF4 data. Reflection intensities were integrated,

corrected for Lorentz and polarisation effects and converted to structure factors using the program CrysAlisPro® (Rigaku Oxford Diffraction), finding 5640 reflections with an R_{int} of

Table 5 Bond lengths (Å) table for utahite*

Cu1–O1	1.975(19)	Te1–O2	1.850(18)	Zn1–O5	1.92(2)
Cu1–O8	1.988(18)	Te1–O5	1.872(19)	Zn1–O4	1.926(18)
Cu1–O6	1.990(19)	Te1–O8	1.954(18)	Zn1–O2	1.972(18)
Cu1–O1	1.998(19)	Te1–O6	1.97(2)	Zn1–O1	2.006(19)
Cu1–O5	2.37(2)	Te1–O7	1.986(17)	<Zn1–O>	1.956
Cu1–O2	2.593(19)	Te1–O7	1.995(17)		
<Cu1–O> _{short}	1.988	<Te1–O>	1.938		
<Cu1–O> _{long}	2.482				
Cu2–O6 (× 2)	1.97(2)	Te2–O9 (× 2)	1.891(18)	Mg1–OW1 (× 2)	2.06(2)
Cu2–O8 (× 2)	1.980(18)	Te2–O4 (× 2)	1.919(18)	Mg1–OW2 (× 2)	2.10(2)
Cu2–O7 (× 2)	2.551(17)	Te2–O3 (× 2)	1.961(19)	Mg1–OW3 (× 2)	2.11(2)
<Cu2–O> _{short}	1.975	<Te2–O>	1.924	<Mg1–O>	2.09
<Cu2–O> _{long}	2.551				
Cu3–O4 (× 2)	1.902(18)	O···O distances		O···O distances	
Cu3–O9 (× 2)	1.912(18)	OW1···O8	2.78	OW3···O3	2.67
Cu3–OW3 (× 2)	2.95(2)	OW1···O9	2.76	OW3···O6	2.79
<Cu3–O> _{short}	1.907	OW2···O7	2.80	O1···O9	2.67
<Cu2–O> _{long}	2.95	OW2···OW3	2.98	O3···O2	2.75

*Cu1:Zn1 occupancy fixed at 95:5, Cu3:Na1 occupancy fixed at 88:12 and Te2/Sb1 occupancy fixed at 99:1

Table 6 Bond valence sums (in valence units, vu) for utahite

Atom	Cu1*	Cu2	Cu3*	Te1*	Te2	Zn2	Mg1	H (calc)	Σ	Assignment
O1	0.45, 0.42					0.43		0.86	2.15	OH
O2	0.08			1.14		0.47			1.74	O
O3					0.93 ($\times 2 \downarrow$)			0.86, 0.06	1.85	OH
O4			0.54 ($\times 2 \downarrow$)		1.00 ($\times 2 \downarrow$)	0.53			2.08	O
O5	0.15			1.09		0.54			1.78	O
O6	0.43	0.45 ($\times 2 \downarrow$)		0.92				0.05	1.84	O
O7		0.09 ($\times 2 \downarrow$)		0.89, 0.88				0.05	1.90	O
O8	0.43	0.44 ($\times 2 \downarrow$)		0.94				0.05	1.86	O
O9			0.53 ($\times 2 \downarrow$)		1.05 ($\times 2 \downarrow$)			0.05, 0.06	1.69	O
OW1							0.36 ($\times 2 \downarrow$)	0.86 ($\times 2 \rightarrow$)	2.08	OW
OW2							0.33 ($\times 2 \downarrow$)	0.86 ($\times 2 \rightarrow$)	2.04	OW
OW3			0.03 ($\times 2 \downarrow$)				0.32 ($\times 2 \downarrow$)	0.86 ($\times 2 \rightarrow$), 0.03	2.10	OW
Σ	1.95	1.95	2.20	5.85	5.98	1.97	2.02			

Values refined using the parameters of Gagné and Hawthorne (2015) for all M–O bonds except Te^{6+} –O bonds (Mills and Christy 2013), Sb^{5+} –O bonds (Mills et al. 2009b), Na–O (Adams 2001) and H–O (Brown 2002). H–O bond-valences calculated using the O...O distances in Table 5, using an ideal 0.95 Å bond length (0.86 vu). H contribution listed in a pooled H (calc) column as individual H sites could not be located

*Cu1:Zn1 occupancy fixed at 95:5, Cu3:Na1 occupancy fixed at 88:12 and Te2/Sb1 occupancy fixed at 99:1

The bold text highlights the bond valence sum values to make them stand out from individual bond valences

0.0959. Structure solution in $P-1$ was carried out using SHELXT (Sheldrick 2015a). Structure refinement by full-matrix least-squares was implemented by SHELXL (Sheldrick 2015b), using neutral atomic scattering factors. Four reflections with calculated F_o/F_C errors greater than 5.00 were excluded from the final refinement.

Only cation sites were refined anisotropically, except for the channel Mg site which was left isotropic. Thus, the Cu1

site was refined as 95 % Cu and 5 % Zn, the Cu3 site was refined as 88 % Cu and 12 % Na and the Te2 site was refined as 99 % Te and 1 % Sb. The joint-occupancies described here are based on the common substitution of Zn^{2+} for Cu^{2+} , Na^+ for Jahn-Teller distorted Cu^{2+} and the joint-occupancy of Sb^{5+} and Te^{6+} in joëlbruggerite (Mills et al. 2009a). The refinement converged to final R_1 and wR_2 (all data) values of 0.126 and 0.296, respectively. Details of data collection and structure

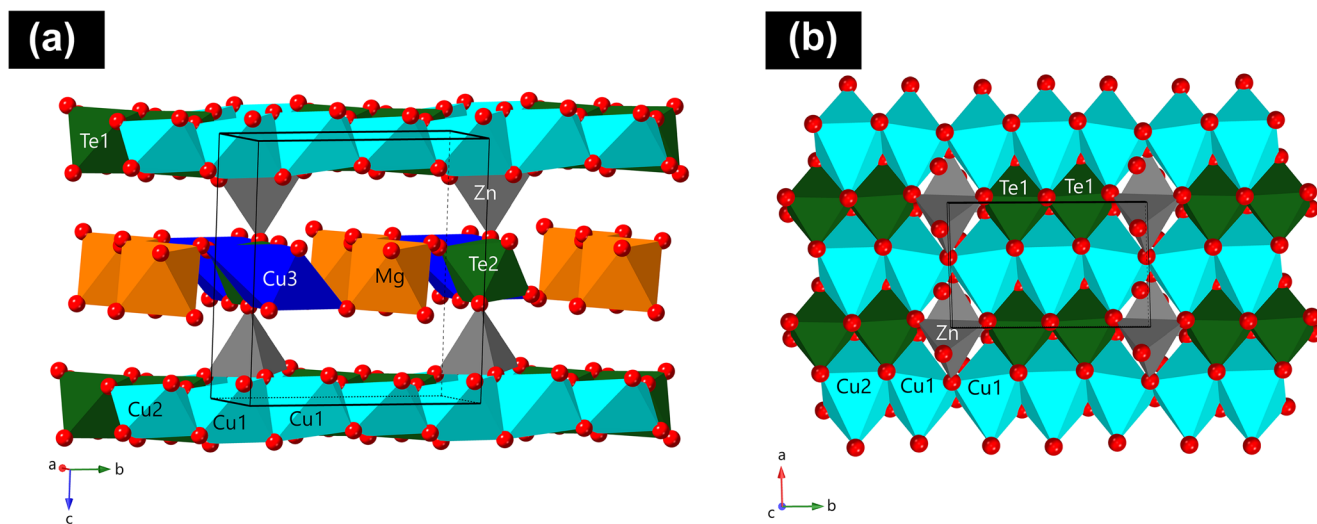


Fig. 3 Crystal structure of utahite in two orientations. $\text{Cu}\phi_6$ polyhedra are in shades of blue, $\text{Te}\phi_6$ octahedra in dark green, $\text{ZnO}_3(\text{OH})$ tetrahedra in grey and $\text{Mg}(\text{H}_2\text{O})_6$ octahedra in orange. **a** Viewed down a , showing layers parallel to the ab plane. Note that the Cu2, Cu1, Cu1 pattern is

repeated *ad infinitum*. Right-hand Cu3 not shown so that Te2 is visible. **b** Layer of the framework viewed down c , with ZnO_4 tetrahedra found above and below the octahedral vacancies

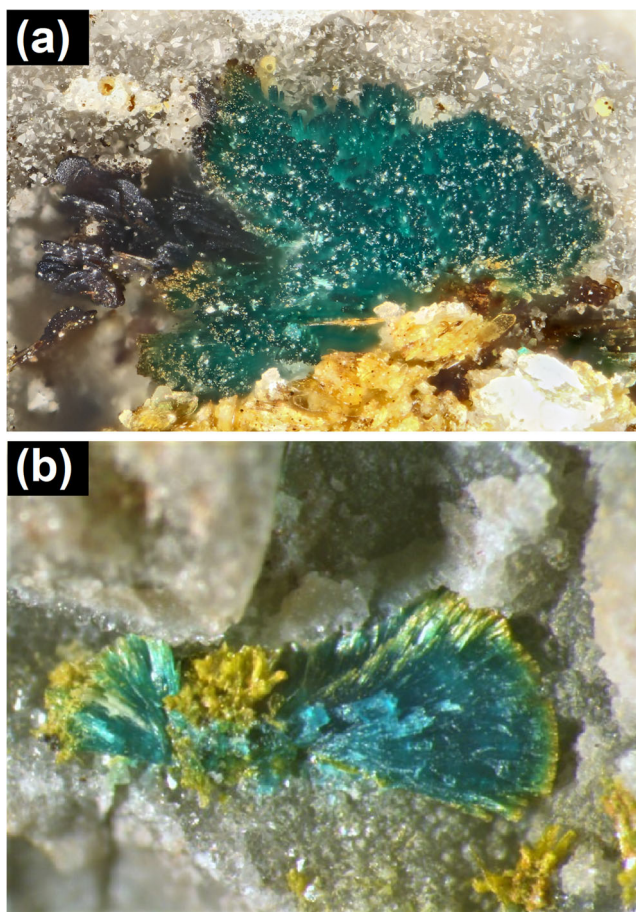


Fig. 4 Utahite (blue) growing in direct association with leisingite (yellow). Both specimens are from Centennial Eureka Mine. **a** Field of view 1 mm, available from <https://www.mindat.org/photo-797227.html>, photo credit Douglas Merson. **b** Field of view 2 mm, available from <https://www.mindat.org/photo-482940.html>, photo credit Brent Thorne

refinement are provided in Table 3. Despite these values being relatively high, all fractional atom coordinates and atom displacement parameters (U^{ij}) as shown in Table 4 result in a chemically sensible structure. Selected bond lengths are provided in Table 5. A bond valence table is provided in Table 6.

Structure description

Utahite has a three-dimensional framework structure (Fig. 3). Jahn-Teller distorted $\text{Cu1O}_4(\text{OH})_2$ octahedra and Cu2O_6 octahedra (in a 2:1 ratio of Cu1- to Cu2-centred octahedra) form ribbons of average composition $[\text{Cu}_{2.67}(\text{OH})_{1.33}]_n$ via edge-sharing along b . Two Te1O_6 octahedra share edges to form $\text{Te1}^{6+}_2\text{O}_{10}$ dimers, which cross-link the $[\text{Cu}_{2.67}(\text{OH})_{1.33}]_n$ ribbons along the a direction, with each $\text{Te1}^{6+}_2\text{O}_{10}$ dimer forming eight edge-sharing links to the $[\text{Cu}_{2.67}(\text{OH})_{1.33}]_n$ ribbons. In vacant sites (one sixth of the octahedral sites in the overall anionic $[\text{Cu}_3\text{Te1}_2\text{O}_8(\text{OH})_4]^{2-}$ layers are vacant), $\text{ZnO}_3(\text{OH})$ tetrahedra sit above and below the plane of the

layers, with three of the tetrahedral vertices to the layers, and one (O4) pointing into the interlayer. This O4 site is an important vertex for both isolated $\text{Te2}^{6+}\text{O}_4(\text{OH})_2$ octahedra and $\text{Cu}_3\text{O}_4(\text{H}_2\text{O})_2$ octahedra, which edge-share with each other to form $[\text{Cu}_3\text{Te}_2\text{O}_4(\text{OH})_2(\text{H}_2\text{O})_2]^{2-}$ chains in the interlayer along a , with linkage to the $[\text{Cu}_3\text{Te1}_2\text{O}_8(\text{OH})_4]^{2-}$ layers through the $\text{ZnO}_3(\text{OH})$ tetrahedra. The $\text{Cu}_3\text{O}_4(\text{H}_2\text{O})_2$ octahedra display the greatest Jahn-Teller distortion of the Cu sites.

Between these chains are the $\text{Mg}(\text{H}_2\text{O})_6$ octahedra, connected to the framework by hydrogen bonds and through the long Cu3–OW3 bonds. Due to the twinned nature of the crystal and high thermal motion of the OW sites, H-atom positions could not be located; however, the O, OH or H_2O character of each O site can be inferred using bond-valence and charge-balance considerations (see Table 6). The OW sites bonded to the Mg site of the $\text{Mg}(\text{H}_2\text{O})_6$ octahedra have an average bond-valence of 0.34 vu , with the remaining valence provided by two O–H bonds. Underbonded O sites around the edge of the channels containing $\text{Mg}(\text{H}_2\text{O})_6$ octahedra gain additional valence from accepting H-bonds donated by the channel H_2O groups.

Additionally, framework O sites with a bond-valence of approximately 1 vu are expected to be OH sites. The O3 site is bonded only to the Te2 site with a Te2–O3 bond-valence of 0.90 vu . O3 points into the interlayer space, providing ample room for the associated H atom. The O1 site, one of the three vertices where the ZnO_4 tetrahedra are connected to the main layers, is the other fully-occupied OH site. These two OH sites (O1 and O3) provide the required 4OH pfu required for charge balance. A small percentage of the other O sites may also be OH sites < 5 % of the time, adding extra charge to compensate for the 12 % Na in the Cu3 site and 1 % Sb in the Te2 site.

Comparison with other te oxy salt structures

The majority of Te^{6+} minerals contain *neso* Te^{6+}O_6 octahedra, with a minority (including utahite) having *soro* non-cyclic clusters or higher connectivity of Te^{6+}O_6 octahedra (Christy et al. 2016). Schieffelinite (Kampf et al. 2012) and chromschieffelinite (Kampf et al. 2012) contain $[\text{Te}^{6+}_2\text{O}_8(\text{OH})_3]^{7-}$ dimers formed from corner-sharing of two $\text{Te}^{6+}\varphi_n$ octahedra, where $\varphi = \text{O}$ or OH. Schieffelinite and chromschieffelinite also contain an additional *neso* $\text{Te}^{6+}\varphi_n$ isolated octahedral unit, $[\text{Te}^{6+}\text{O}_4(\text{OH})_2]^{4-}$ in utahite and $[\text{Te}^{6+}\text{O}_2(\text{OH})_4]^{2-}$ in schieffelinite and chromschieffelinite (Kampf et al. 2012). Thorneite (Kampf et al. 2010) and eckhardtite (Kampf et al. 2013) both have $\text{Te}^{6+}_2\varphi_{10}$ dimers formed from the edge-sharing of two Te^{6+}O_6 octahedra in their structures, but no additional *neso* $\text{Te}^{6+}\varphi_n$ octahedra.

Utahite also has some notable structural similarities to other Cu– Te^{6+} –O minerals from the Centennial Eureka mine. Utahite has been observed growing directly with other Te-oxy salts, especially with leisingite (Fig. 4). The utahite and

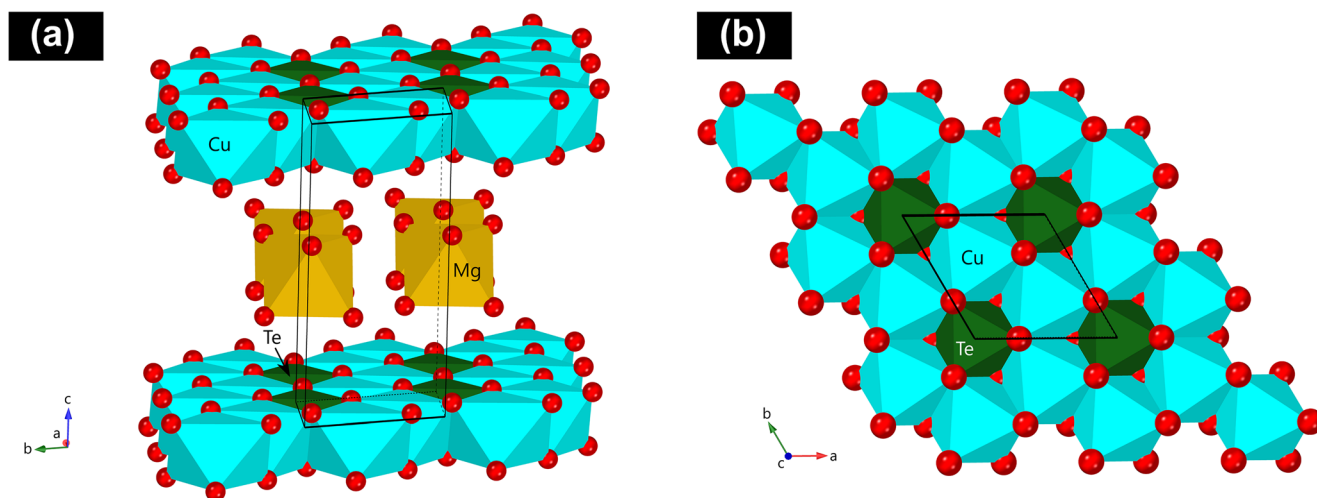


Fig. 5 The crystal structure of leisingite in two orientations. Colour scheme is identical to that used for utahite. **a** Viewed down *a* showing layers parallel to the *ab* plane. **b** Viewed down *c*. Interlayer sites not shown for clarity. Note similarities to utahite

leisingite (Fig. 5) structures are rather similar, in that both have layers composed of $\text{Cu}\phi_6$ and $\text{Te}\phi_6$ octahedra with $\text{Mg}(\text{H}_2\text{O})_6$ octahedra found between the layers (Margison et al. 1997). However, utahite also has additional Te- and Cu-centred polyhedra between the main layers and $\text{ZnO}_3(\text{OH})$ tetrahedra providing linkage to additional interlayer sites, compared to the low-Zn (0.45 wt%) leisingite, which has no Zn-dominant sites. Minerals which grow nearby or overlie each other may have similar crystal structure motifs due to the phenomenon of topotactic growth (Glasser et al. 1962; Marler and Gies 2012; Génin et al. 2012). Topotactic growth has been explored for a variety of minerals and related synthetic compounds, such as silver tellurides (Baumer and Nilges 2017), the complex silicates of the chevkinite group (Galanciak et al. 2020) and most pertinently, in secondary minerals such as arsenates like jeankempite, hypothesised to grow topotactically following the dehydration of underlying guérinite (Olds et al. 2020).

There are likely to be many more Mg–Cu–Zn–Te–O compounds which are yet to be synthesised, or potentially found in Nature. The incorporation of Mg^{2+} into the more commonly studied Cu–Zn–Te–O system would provide a further layer of chemical and structural complexity. For instance, in the synthetic Cu–Zn–Te⁶⁺–O system, $\text{Cu}_5\text{Zn}_4(\text{TeO}_6)_3$ and $\text{Cu}_3\text{Zn}_3(\text{TeO}_6)_2$ have been characterised (Wulff and Müller-Buschbaum 1998) but no compounds with additional Mg^{2+} are known. Three compounds in the Cu–Zn–Te⁴⁺–O system with additional anions (SxO_4^{2-} or Cl^-) have also recently been described, showing the versatility of adding new elements to a system, whether anions or cations (Missen et al. 2020b). This study again shows that there are many more diverse Te–O

crystal structures to be discovered both in Nature and in the laboratory.

Supplementary Information The online version contains supplementary material available at <https://doi.org/10.1007/s00710-021-00746-y>.

Acknowledgements Support funding has been provided to OPM by an Australian Government Research Training Program (RTP) Scholarship, a Monash Graduate Excellence Scholarship (MGES) and a Robert Blackwood Monash-Museums Victoria scholarship. We thank Brendan Abrahams (University of Melbourne) for facilitating the single-crystal X-ray diffraction study and carrying out the initial data processing. Tony Steede (Royal Ontario Museum) is thanked for his helpful advice on the Raman study. Tanya Kizovski (Royal Ontario Museum) is thanked for her assistance in collecting the preliminary Raman spectrum and Katherine Dunnell (Royal Ontario Museum) is thanked for her role in loaning the ROM specimen. Graham Hutchinson (University of Melbourne) is thanked for his assistance with the microprobe measurements on the ROM specimen. We thank Douglas Merson and Brent Thome for authorising us to use their photos of leisingite with utahite. Finally, we thank Joël Brugger (Monash University) for his comments and PhD supervision support of OPM.

References

- Adams S (2001) Relationship between bond valence and bond softness of alkali halides and chalcogenides. *Acta Cryst B* 57:278–287
- Baumer F, Nilges T (2017) A chemical, high-temperature way to $\text{Ag}_{1.9}\text{Te}$ via quasi-topotactic reaction of stuetzite-type $\text{Ag}_{1.54}\text{Te}$: structural and thermoelectric properties. *Inorg Chem* 56:13930–13937
- Brown ID (2002) *The chemical bond in inorganic chemistry*. Oxford University Press, Oxford, p 230
- Christy AG, Mills SJ, Kampf AR (2016) A review of the structural architecture of tellurium oxycompounds. *Min Mag* 80:415–545

- Gagné OC, Hawthorne FC (2015) Comprehensive derivation of bond-valence parameters for ion pairs involving oxygen. *Acta Cryst B* 71: 562–578
- Galanciak J, Bagiński B, Macdonald R, Belkin HE, Kotowski J, Jokubauskas P (2020) Relationships between monazite, apatite and chevkinite-group minerals in the rhyolitic Joe Lott Tuff, Utah, USA. *Lithos* 354–355:105349
- Génin J-MR, Guérin O, Herbillon AJ, Kuzmann E, Mills SJ, Morin G, Ona-Nguema G, Ruby C, Upadhyay C (2012) Redox topotactic reactions in Fe^{II-III} (oxy)hydroxycarbonate new minerals related to fougèrite in gleysols: “trébeurdenite and mössbauerite”. *Hyperfine Interact* 204:71–81
- Glasser LSD, Glasser FP, Taylor HFW (1962) Topotactic reactions in inorganic oxy-compounds. *Quart Rev Chem Soc* 16:343–360
- Grice JD, Roberts AC (1995) Frankhawthorneite, a unique HCP framework structure of a cupric tellurate. *Can Min* 33:649–654
- Grice JD, Groat LA, Roberts AC (1996) Jensenite, a cupric tellurate framework structure with two coordinations of copper. *Can Min* 34:55–59
- Kampf AR, Housley RM, Marty J (2010) Lead-tellurium oxysalts from Otto Mountain near Baker, California: III Thorneite, Pb₆(Te⁶⁺ +₂O₁₀)(CO₃)Cl₂·H₂O, the first mineral with edge-sharing octahedral tellurate dimers. *Am Mineral* 95:1548–1553
- Kampf AR, Mills SJ, Housley RM, Rumsey MS, Spratt J (2012) Lead-tellurium oxysalts from Otto Mountain near Baker, California: VII Chromschiefelinite, Pb₁₀Te⁶⁺ +₆O₂₀(OH)₁₄(CrO₄)·5H₂O, the chromate analog of schiefelinite. *Am Mineral* 97:212–219
- Kampf AR, Mills SJ, Housley RM, Rossman GR, Marty J, Thorne B (2013) Lead-tellurium oxysalts from Otto Mountain near Baker, California: XI Eckhardite, (Ca,Pb)CuTe⁶⁺O₅·H₂O, a new mineral with HCP stair-step layers. *Am Mineral* 98:1617–1623
- Libowitzky E (1999) Correlation of O-H stretching frequencies and O-H···O hydrogen bond lengths in minerals. *Monatsh Chem* 130: 1047–1059
- Margison SM, Grice JD, Groat LA (1997) The crystal structure of leisingite, (Cu²⁺,Mg,Zn)₂(Mg,Fe)Te⁶⁺O₆·6H₂O. *Can Mineral* 35: 759–763
- Marler B, Gies H (2012) Hydrous layer silicates as precursors for zeolites obtained through topotactic condensation: a review. *Eur J Mineral* 24:405–428
- Mills SJ, Christy AG (2013) Revised values of the bond-valence parameters for Te^{IV}-O, Te^{VI}-O and Te^{IV}-Cl. *Acta Crystallogr Sect B* 69:145–149
- Mills SJ, Kolitsch U, Miyawaki R, Groat LA, Poirier G (2009a) Joëlbruggerite, Pb₃Zn₃(Sb⁵⁺,Te⁶⁺)As₂O₁₃(OH,O), the Sb⁵⁺ analog of dugganite, from the Black Pine mine, Montana. *Am Mineral* 94: 1012–1017
- Mills SJ, Christy AG, Chen EC-C, Raudsepp M (2009b) Revised values of the bond valence parameters for ⁶¹Sb(V)-O and ¹²¹Sb(III)-O. *Z Kristallogr* 224:423–431
- Missen OP, Ram R, Mills SJ, Etschmann B, Reith F, Shuster J, Smith DJ, Brugger J (2020a) Love is in the Earth: a review of tellurium (bio)geochemistry in Earth surface environments. *Earth Sci Rev* 204:103150
- Missen OP, Weil M, Mills SJ, Libowitzky E, Kolitsch U, Stöger B (2020b) The crystal structures of three new copper-zinc oxotellurates(IV). *Z Anorg Allg Chem* 646:476–488
- Olds TA, Kampf AR, Dal Bo F, Bums PC, Guo X, McCloy JS (2020) Jeankempite, Ca₅(AsO₄)₂(AsO₃OH)₂(H₂O)₇, a new arsenate mineral from the Mohawk Mine, Keweenaw County, Michigan, USA. *Mineral Mag* 84:959–969
- Pekov IV, Jensen MC, Roberts AC, Nikischer AJ (2010) A new mineral from an old locality: Eureka dumpite takes seventeen years to characterize. *Mineral News* 26:1–3
- Pekov IV, Chukanov NV, Zadov AE, Roberts AC, Jensen MC, Zubkova NV, Nikischer AJ (2011) Eureka dumpite, (Cu, Zn)₁₆(TeO₃)₂(AsO₄)₃Cl(OH)₁₈·7H₂O, a new supergene mineral species. *Geol Ore Deposits* 53:575–582
- Roberts AC, Ercit TS, Cureton FF (1994) Mcalpineite, Cu₃TeO₆·H₂O, from the McAlpine mine, Tuolumne County, California, and from the Centennial Eureka mine, Juab County, Utah. *Mineral Mag* 58: 417–424
- Roberts AC, Grice JD, Criddle AJ, Jensen MC, Harris DC, Moffatt EA (1995) Frankhawthorneite, Cu₂Te⁶⁺O₄(OH)₂, a new mineral species from the Centennial Eureka Mine Tintic District, Juab County, Utah. *Can Mineral* 33:641–647
- Roberts AC, Grice JD, Groat LA, Criddle AJ, Gault RA, Erd RC, Moffatt EA (1996a) Jensenite, Cu₃Te⁶⁺O₆·2H₂O, a new mineral species from the Centennial Eureka Mine, Tintic District, Juab County, Utah. *Can Mineral* 34:49–54
- Roberts AC, Groat LA, Grice JD, Gault RA, Jensen MC, Moffatt EA, Stirling JA (1996b) Leisingite, Cu(Mg,Cu,Fe,Zn)₂Te⁶⁺O₆·6H₂O, a new mineral species from the Centennial Eureka mine, Juab County, Utah. *Mineral Mag* 60:653–658
- Roberts AC, Stirling JA, Criddle AJ, Jensen MC (1997a) Utahite, a new mineral and associated copper tellurates from the Centennial Eureka Mine, Tintic District, Juab County, Utah. *Mineral Rec* 28:175–179
- Roberts AC, Gault RA, Jensen MC, Criddle AJ, Moffatt EA (1997b) Juabite, Cu₅(Te⁶⁺O₄)₂(As⁵⁺O₄)₂·3H₂O, a new mineral species from the Centennial Eureka mine, Juab County, Utah. *Mineral Mag* 61: 139–144
- Sheldrick GM (2015a) SHELXT—Integrated space-group and crystal-structure determination. *Acta Cryst A* 71:3–8
- Sheldrick GM (2015b) Crystal structure refinement with SHELXL. *Acta Cryst C* 71:3–8
- Wulff L, Müller-Buschbaum H (1998) Zur Kristallchemie der Kupfer(II)-Zinktellurate Cu₅Zn₄Te₃O₁₈ und Cu_{1,5}Zn_{1,5}TeO₆, mit einer Notiz über Cu_{1,5}Co_{1,5}TeO₆ / On the Crystal Chemistry of the Copper(II) Zinc Tellurates Cu₅Zn₄Te₃O₁₈ and Cu_{1,5}Zn_{1,5}TeO₆ with a Note on Cu_{1,5}Co_{1,5}TeO₆. *Z Naturforsch B53*:53–57

Publisher's note Springer Nature remains neutral with regard to jurisdictional claims in published maps and institutional affiliations.